

## The Taylor–Green Vortex and Fully Developed Turbulence

M. E. Brachet,<sup>1</sup> D. Meiron,<sup>2</sup> S. Orszag,<sup>3</sup> B. Nickel,<sup>4</sup> R. Morf,<sup>5</sup> and U. Frisch<sup>1</sup>

*Received November 29, 1983*

---

We here report results obtained from numerical simulations of the Taylor–Green three-dimensional vortex flow. This flow is perhaps the simplest system in which one can study the generation of small scales by three-dimensional vortex stretching and the resulting turbulence. The problem is studied by both direct spectral numerical solution of the Navier–Stokes equations (with up to  $256^3$  modes) and by power series analysis in time.

The inviscid dynamics are strongly influenced by symmetries which confine the flow to an impermeable box with stress-free boundaries. There is an early stage during which the flow is strongly anisotropic with well-organized (laminar) small-scale excitation. The flow is smooth but has complex-space singularities within a distance  $\delta(t)$  of the real space which are manifest through an exponential tail in the energy spectrum. It is found that  $\delta(t)$  decreases exponentially in time to the limit of our resolution. Indirect evidence is presented that more violent vortex stretching takes place at later times, possibly leading to a real singularity ( $\delta = 0$ ) at a finite time. These direct integration results are consistent with new presented results extending the Morf, Orszag, and Frisch temporal power series analysis from order  $t^{40}$  to order  $t^{80}$ . Still, convincing evidence for or against the existence of a real singularity will require even more sophisticated analysis.

The viscous dynamics (decay) have been studied for Reynolds numbers  $R$  (based on integral scale) up to 3000 and beyond the time  $t_{\max}$  at which the

---

Work supported by the NSF under grants Nos. ATM-8017284 and DMR-77-10210; by the Office of Naval Research under Contracts N00014-77-C-0138 and N00014-79-C-0478; by the NSERC of Canada; and by the A. P. Sloan Foundation.

<sup>1</sup> CNRS, Observatoire de Nice, 06300 Nice, France.

<sup>2</sup> Department of Mathematics, California Institute of Technology, Pasadena, California 91125.

<sup>3</sup> Department of Mathematics, MIT, Cambridge, Massachusetts 02139.

<sup>4</sup> Schlumberger-Doll Research, Ridgefield, Connecticut 06877.

<sup>5</sup> Laboratories RCA Ltd., Zurich, Switzerland.

maximum energy dissipation is achieved. Early time, high  $R$  dynamics are essentially inviscid and laminar. Then, instabilities starting at small scales, which may be driven by viscosity, make the flow increasingly chaotic (turbulent) with extended high-vorticity patches appearing away from the impermeable walls. Near  $t_{\max}$  the small scales of the flow are nearly isotropic provided  $R \gtrsim 1000$ . Various features characteristic of fully developed turbulence are observed near  $t_{\max}$  when  $R = 3000$ .

---

**KEY WORDS:** 2.70, 3.40G, 47.10, 47.25C.

## INTRODUCTION

Viscous incompressible three-dimensional flow can become turbulent when the Reynolds number  $R$  is sufficiently large. The latter is determined by the typical length scale  $L$  of the flow, a typical velocity  $V$ , and the kinematic viscosity  $\nu$ , as the ratio of the viscous diffusion time  $L^2/\nu$  to the circulation (turnover) time  $L/V$ .

In this paper we shall be concerned with the properties of flows at very large Reynolds numbers. In contrast to the situation at the onset of turbulence, where in general excitation is only in the large scales of the flow and where the dynamics appears to be governed by the interaction of only a few modes,<sup>(1)</sup> high Reynolds number turbulence involves excitation in a very wide range of scales.

In fact, Fourier analysis of velocity signals from a probe in high Reynolds number flow (e.g., turbulent jet) reveals the kind of energy spectrum shown in Fig. 1. The spectrum follows a power law of the form  $k^{-m}$  ( $m \approx 5/3$ ) over a range of scales (i.e., inverse wavenumbers  $k$ ) extending from the integral scale  $l_0$  to the dissipation scale  $l_D$ . The range of scales  $l \sim l_0$  is called the energy-carrying or production range because that is where most of the turbulent energy is produced (usually by some instability mechanism). The range  $l_0 \gg l \gg l_D$  is called inertial range because the dynamics is dominated here by the inertial terms in the Navier–Stokes equation (direct production and dissipation are negligible). The range of scales  $l < l_D$  is called the dissipation range because dissipation terms as well as inertial terms are relevant here.

As the Reynolds number increases the dissipation range moves to larger wave numbers, in fact, the ratio  $l_0/l_D$  is experimentally found to increase like  $R^n$  ( $n \approx 3/4$ ) and in the limit of infinite Reynolds number a power law spectrum extending to infinite wavenumbers will result.

While all this was predicted in 1941 by Kolmogorov<sup>(2)</sup> there still remains a major lack in theoretical understanding: In fact, the Kolmogorov theory is inconsistent with another important experimental observation: the

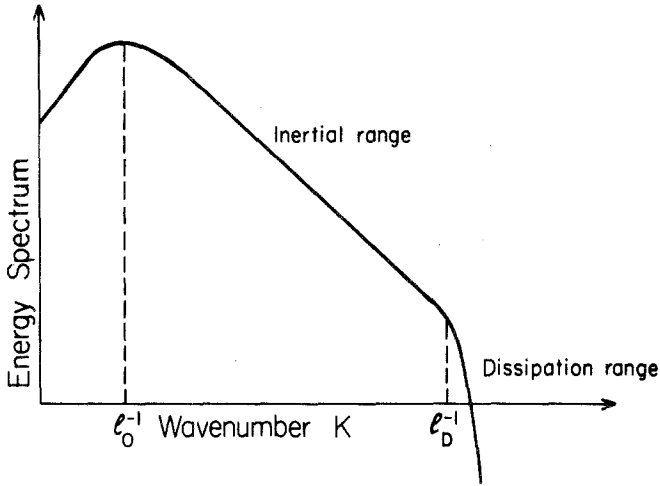


Fig. 1. Energy-spectrum of high Reynolds number turbulence in log-log scale.  $l_0$  is the integral scale and  $l_D$  is the dissipation scale.

fact that small-scale activity is intermittent.<sup>(3)</sup> Indeed, high-pass filtering of turbulent signals shows that small-scale activity comes in bursts. Intermittency appears both in the inertial and in the dissipation range. Inertial range intermittency has not received any systematic explanation. There have been attempts to modify the original Kolmogorov (1941) theory in order to include the effects of intermittency,<sup>(4-6)</sup> but the problem is still open (cf. Ref. 7). Dissipation range intermittency is much better understood<sup>(8)</sup> and has been related to singularities of the solutions to the Navier–Stokes equation at complex times.<sup>(7,9)</sup>

The essence of the explanation is that high-pass filtering of an analytic function with complex-time singularities produces bursts centered at the real part of the singularity position and with overall amplitude proportional to  $\exp(-\Omega|\tau|)$  where  $\Omega$  is the high-pass filter frequency and  $\tau$  the imaginary part of the singularity. The rare singularities closest to the real time axis dominate for large  $\Omega$ . A similar consideration can be applied to the connection between the small-scale (large wavenumber  $k$ ) behavior of the energy spectrum and complex space singularities of the velocity field. In this view, the exponential decay rate, characterized by the cutoff wavenumber  $k_D \approx 1/l_D$ , would be associated with the distance from the real domain of the singularities in complex space, and in the limit of infinite Reynolds number one might then expect that singularities would occur at real points in space and thus lead to a power law spectrum for all  $k$ , whose exponent would be associated with the spatial structure of the flow in the

vicinity of a real space singularity. This mechanism actually works for solutions of the Burgers equation

$$\partial_t V + V \partial_x V = \nu \partial_{xx} V \quad (1)$$

which in the zero-viscosity limit ( $\nu = 0$ ) undergo the formation of shocks, thus leading to a power law  $E(k) \propto k^{-2}$  for the energy spectrum.<sup>(10)</sup>

For the Navier–Stokes equation (or for  $\nu = 0$ , the Euler equation) the situation is, however, quite different: For the two-dimensional Euler equations (i.e., even in the inviscid case!) it has been proven that real singularities will never occur unless present initially (cf. Ref. 7). Less is known for the three-dimensional case, where in contrast to the two-dimensional case, the generation of small scales occurs by three-dimensional vortex stretching and vortex lines could conceivably be stretched to infinite length.

These considerations have motivated our study of one particular three-dimensional flow, the Taylor–Green vortex flow.<sup>(11)</sup> A full account of this work has been published recently<sup>(12)</sup> and we shall review the principal results here.

The Taylor–Green vortex is that three-dimensional flow that develops from the single-Fourier mode initial condition

$$\begin{aligned} V_x(x, y, z) &= \sin x \cos y \cos z \\ V_y(x, y, z) &= -\cos x \sin y \cos z \\ V_z &\equiv 0 \end{aligned} \quad (2)$$

under the action of the Navier–Stokes equation

$$\partial_t \mathbf{V} + \mathbf{V} \cdot \nabla \mathbf{V} = -\nabla p + \nu \nabla^2 \mathbf{V} \quad (3)$$

together with the condition of incompressibility  $\nabla \cdot \mathbf{V} = 0$ . While the initial symmetry  $V_y(x, y, z) = V_x(y, \pi - x, z)$  holds for all later times, the  $z$  component of the velocity field becomes nonzero for all  $t > 0$  and the flow becomes truly three-dimensional. However, owing to the symmetries computational work and data storage is significantly less than in the general nonsymmetric case and thus computations with higher spatial resolution become possible. This allows flow studies at much higher Reynolds numbers than is possible in the general nonsymmetric case.<sup>6</sup> On the other hand, the fact that the initial condition contains one single Fourier mode allows the computation of temporal power series for the velocity field

$$\mathbf{V}(\mathbf{r}, t) = \sum_{p=0}^{\infty} t^p \mathbf{V}^{(p)}(\mathbf{r}) \quad (4)$$

<sup>6</sup> A Taylor Green code with resolution of  $(256)^3$  Fourier modes requires roughly an equivalent amount of computation as a general spectral code with resolution  $(64)^3$ .

where  $\mathbf{V}^{(p)}$  can be obtained by recursion from the Navier–Stokes equation in a finite number of steps. This series representation will converge for short times (cf. Ref. 7 and references therein) and can be used for the calculation of spatial averages such as the mean square vorticity (or enstrophy)  $\Omega(t)$

$$\Omega(t) = \frac{1}{2} \sum_{\mathbf{k}} |\mathbf{k}|^2 \mathbf{u}(\mathbf{k}, t) \quad (5)$$

with a temporal power series

$$\Omega(t) = \sum_{n=0}^{\infty} A_n t^n \quad (6)$$

The Fourier transform of the velocity field has been denoted by  $\mathbf{u}(\mathbf{k}, t)$ . Again the computation of the coefficients  $A_n$  up to an order  $n_{\max}$  involves a finite number of Fourier modes and can be calculated in a finite number of recursion steps using the Navier–Stokes equation. Clearly, the development of a power law energy spectrum at a finite time  $t_*$  would imply a singularity for  $\Omega(t)$  at  $t_*$  and therefore the behavior of the Taylor series (6) for  $\Omega$  will be of great interest for the analysis of small scale structure in the flow. This method together with direct numerical integration of the Navier–Stokes equation has been utilized in our work. In Section 2 we shall review results for the inviscid flow and Section 3 will be devoted to finite Reynolds number results.

## 2. ANALYSIS OF INVISCID FLOW

We begin our discussion with results based on temporal power series calculations for  $\Omega(t)$  [Eq. (6)]. A computation of this series up to order  $t^{44}$  was carried out by Morf, Orszag, and Frisch.<sup>(13)</sup> The radius of convergence was found to be determined by imaginary time singularities at  $t^2 \approx -5.7$ . Analytic continuation was required to study the question of the existence of a real time singularity. Padé approximants indicated the possibility of a singularity at  $t \approx 5.2$ . The reliability of this method was subsequently studied for flow problems for which rigorous results are known.<sup>(14)</sup> In particular, for the inviscid Burgers equation, series-extrapolation methods correctly predict locations and nature of the singularity, corresponding to the formation of shock waves. Also, for two-dimensional Euler flow, series analysis does not predict a real singularity, consistent with rigorous theorems.<sup>(15)</sup> In the present work, we have extended the power series for  $\Omega(t)$  up to order  $t^{80}$ . This was possible through efficient use of fast Fourier transform methods for the recursive calculation of  $\mathbf{V}^{(p)}(\mathbf{r})$  (4) [together with multiple precision (28 hexadecimal mantissa) arithmetic]. Padé,  $D \log$

<sup>7</sup> Note that for  $\nu = 0$  the series (6) contains only even terms and is analyzed in the variable  $t^2$ .

**Table I. Singularities and Estimates of  $d\Omega/dt$  from Padé Approximants**

Approximant	Complex- $t^2$ plane pole locations with $( \arg t^2  < \frac{1}{4} \pi)$		$\frac{d\Omega}{dt} \Big _{t=4}$
[17/22]	18.94,	$16.58 \pm 11.33i$	3.98
[18/21]	20.53,	$15.84 \pm 7.89i$	3.16
[19/20]	31.32,	$15.65 \pm 4.43i$	2.03
[20/19]	31.12,	$15.66 \pm 4.45i$	2.04
[21/18]	—	$14.94 \pm 3.19i$	1.23
[19/22]	20.05,	$15.66 \pm 8.54i$	3.32
[19/21]	19.95,	$15.56 \pm 8.64i$	3.35
[21/19]	18.50,	$14.29 \pm 7.35i$	3.91
[22/18]	—	$15.76 \pm 4.05i$	1.87

Padé,<sup>(16)</sup> and inhomogeneous differential approximants<sup>(17)</sup> suggest singularities of  $\Omega$  at  $t^2 = -4.65 \pm 0.05$  and at  $t^2 = (1.5 \pm 0.2) \pm (5.4 \pm 0.2)i$ , implying a radius of convergence  $R_c \approx 2.16$ . An additional singularity appears to be present at  $|t^2| \approx 15\text{--}20$  either on the positive real axis or as a nearby complex-conjugate pair. The uncertainty in the nature of this singularity is illustrated in Table I, in which we give a partial list of Padé approximants of  $\Omega$  with all pole locations with  $|\arg t^2| < \frac{1}{4} \pi$ .

Since in most cases the poles shown in Table I are also the poles furthest from the origin, their almost “random” position is not so surprising. We believe that this randomness is attributable to a lack of information, i.e., the limited number of coefficients available. This conclusion is based on the observation that approximants determined from a series up to  $t^{78}$  typically predict the coefficient of the term of order  $t^{80}$  to 7-digit accuracy, whereas the computed coefficient, we believe, has three more significant digits. In addition, the lack of understanding of the unphysical singularities of seriously hampers our attempts to deduce its analytic structure at real times.

Let us now turn to the results based on direct integration of the Euler equation (or Navier–Stokes equation for zero viscosity). In order to probe the small-scale structure of the flow we look at the time evolution of the spherically averaged energy spectrum  $E(k, t)$  calculated as the band average

$$E(k, t)\Delta k = \frac{1}{2} \sum_{\mathbf{k}' \in C(k)} |\mathbf{u}(\mathbf{k}', t)|^2 \tag{7}$$

$$C(k) = \{\mathbf{k}' \mid k - \frac{1}{2}\Delta k \leq |\mathbf{k}'| < k + \frac{1}{2}\Delta k\}.$$

In Figs. 2 and 3 we plot the energy spectrum both in linear–log and log–log

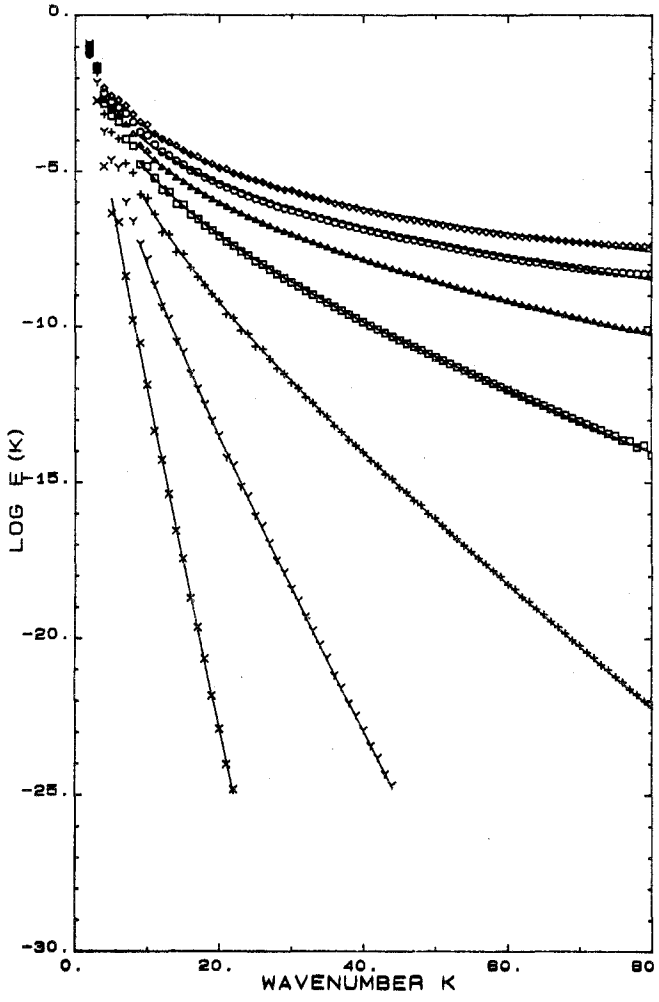


Fig. 2. The inviscid spectrum  $E(k, t)$  in log-linear scale. The different symbols distinguish the spectra at equally spaced times, from crosses at  $t = 0.5$  to diamonds at  $t = 3.5$ .

scales for the times  $t = 0.5, 1, 1.5, 2, 2.5, 3,$  and  $3.5$ . While the early-time behavior is essentially exponential, for times  $t \gtrsim 2.5$  a power law regime is conspicuous. Fitting the energy spectrum to the form

$$E(k, t) = A(t)k^{-n(t)}e^{-2\delta(t)k} \tag{8}$$

we obtain the solid lines in Figs. 2 and 3. While the exponent of the power

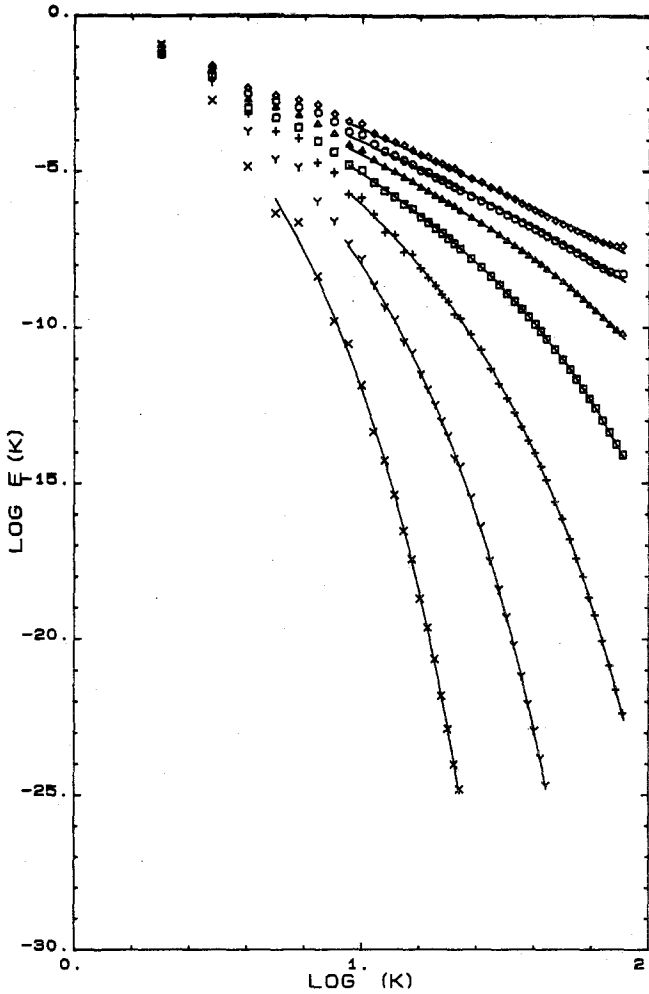


Fig. 3. The inviscid spectrum  $E(k, t)$  in log-log scale. Symbols are the same as in Fig. 2.

law part varies little with time and approaches the value  $n(t) \approx 4$  for  $t > 2$ , the cutoff wave vector  $k_c = (2\delta)^{-1}$  increases exponentially with time in the form

$$k_c(t) \approx k_c(0)e^{t/T} \tag{9}$$

with a time constant  $T \approx 0.57$ , which corresponds to a doubling time  $\Delta t \approx 0.40$ . Equation (9) holds up to the limit of resolution which for our  $(256)^3$ -computation occurs for  $k_c(t) \approx k_{max} = 84$ . This actually occurs al-

ready at a time of 2.5. The variable  $\delta(t)$  of Eq. (8) which is proportional to  $k_c^{-1}$  may be regarded as the width of the analyticity strip of the velocity field  $\mathbf{V}(\mathbf{z}, t)$  in complex  $\mathbb{C}^3$  ( $\mathbf{z} = \mathbf{x} + i\mathbf{y}$ ,  $\mathbf{x}$  and  $\mathbf{y} \in \mathbb{R}^3$ ).<sup>(18,7)</sup> The result (9) thus implies that singularities of the velocity field would approach the real domain in an exponential manner never actually hitting it, but coming arbitrarily close. This would thus imply that no finite time singularity exists in this flow. This conclusion is, however, based on the assumption that no crossover in the evolution of the flow occurs. However, as discussed in great detail in Ref. 12 there is strong evidence that such crossover does occur in the flow. It is based on the numerically observed growth of the strain rate (or convergence) near the special point  $x = z = \pi/2$ ,  $y = 0$ . It is pointed out that the behavior of the flow field near this point will for  $t \gtrsim 3$  dominate the large  $k$  behavior of the spectrum actually giving rise to significantly more rapid growth of the cutoff wave number  $k_c(t)$  with a doubling time of the order  $\Delta t' \approx 0.2$  around  $t = 4$ .

Finally it is interesting to compare the results of direct integration with those based on series extrapolation techniques and test in this way the reliability of the Padé extrapolation. A detailed comparison is made in Ref. 12. It is found that up to a time  $t \approx 3.6$  the results for  $\Omega(t)$  and  $d\Omega/dt$  based on integration are consistent with those based on series extrapolation. In other words there is agreement significantly beyond the radius of convergence ( $R_c \approx 2.16$ ). In addition, it is interesting to note that the results for  $d\Omega/dt$  at  $t = 4$ , which are for resolutions  $(64)^3$ ,  $(128)^3$ , and  $(256)^3$ :  $(d\Omega/dt)$  ( $t = 4$ ) = 1.53, 2.06, and 2.59, respectively, are consistent with all Padé approximants which exhibit a singularity at around  $t^2 \approx 18$ –20 (cf. Table I), based on the plausible assumption that the integration results are lower bounds to the true value of  $d\Omega/dt$  at  $t = 4$ .

This is the strongest evidence we have at present for the existence of a real-time singularity and its possible time of occurrence  $t_* \approx 4.4 \pm 0.2$ . Although the above argument is by no means definitive, it does serve as an excellent example of the complementary nature of the time-series and time-marching techniques used here.

To conclude this section, we should like to discuss a possible explanation for the complicated nature of series (6), as evidenced by the “noise” in the Padé analysis. Indeed, systems have been studied which naturally display that kind of “noise,” which results from the existence of natural boundaries in these systems. A well-studied example is the Hénon–Heiles system which has been found to exhibit natural boundaries with a self-similar fractal structure.<sup>(19,20)</sup> Such a structure, one may speculate, might result in the Taylor–Green vortex if the flow develops into an infinite cascade of ever smaller vortices, and no method of extrapolation from a finite number of Taylor coefficients might ever work.

### 3. HIGH-REYNOLDS-NUMBER BEHAVIOR

Here, we report results obtained by numerical solution of the viscous Navier–Stokes equation for the Taylor–Green vortex flow. We will only give a brief summary and refer the reader to the detailed discussion of Ref. 12, which contains also a great number of illuminating flow pictures.

The Reynolds number is  $R = 1/\nu$ , noting that the length and velocity scales of the initial flow are of order unity. While the inviscid runs cannot be extended accurately beyond  $t \approx 3$ , finite  $R$  runs may be accurate for all times. For example the  $(256)^3$  calculation is accurate for all but the smallest dissipation scale for  $R \lesssim 3000$ .

The time evolution of the energy dissipation  $\epsilon(t) = 2\nu\Omega(t)$  is plotted versus  $t$  in Fig. 4 for  $100 \leq R \leq 3000$ . The observed enhancement of mean-square vorticity  $\Omega(t)$  for short times measures the strength of nonlinear vortex stretching while the late-time decay of  $\epsilon(t)$  reflects the decay of the flow by viscous damping. The results also show that the maximum enstrophy  $\Omega_{\max}$  is roughly proportional to  $R$ , since the maximum dissipa-

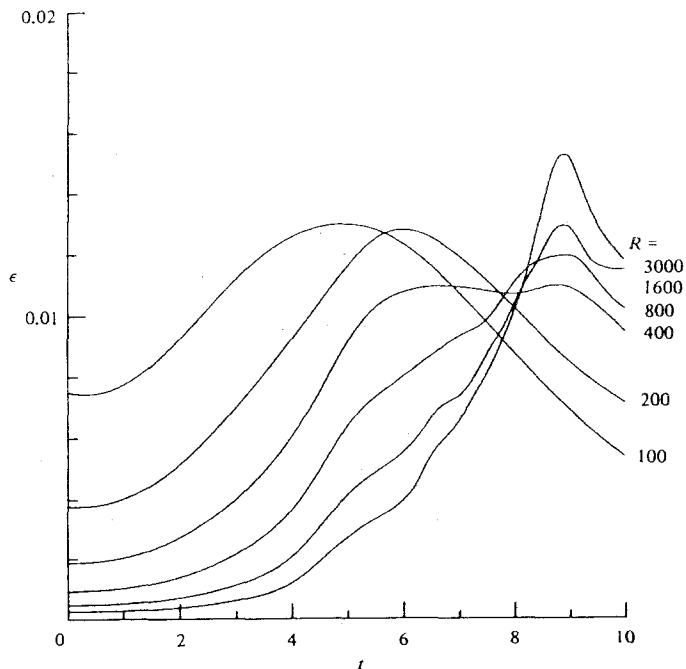


Fig. 4. Rate of energy dissipation  $\epsilon(t) = 2\nu\Omega(t)$  vs.  $t$  for  $100 \leq R \leq 3000$ . Note that the time  $t_{\max}$  of maximum dissipation is shifted from  $t_{\max} \approx 7$  at  $R = 200$  to  $t_{\max} \approx 9$  at  $R = 3000$ .

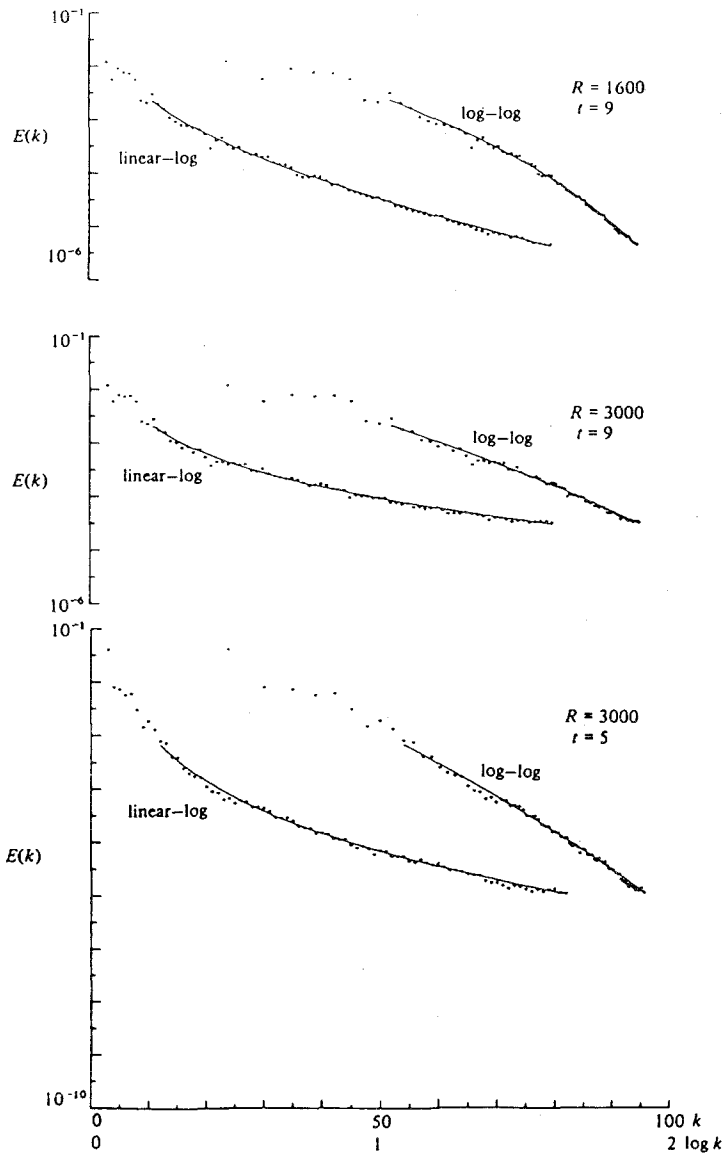


Fig. 5. Plots of energy spectra  $E(k)$  vs.  $k$  on linear-log and log-log scales: bottom:  $t = 5$ ,  $R = 3000$ ; middle:  $t = t_{\max} \approx 9$ ,  $R = 3000$ ; top:  $t = t_{\max}$ ,  $R = 1600$ . The solid lines represent fits using Eq. (8).

tion varies only weakly with  $R$ . The time  $t_{\max}$  at which the dissipation reaches its maximum depends only weakly on  $R$  up to  $R \approx 300$ , until at  $R \approx 400$  a second maximum appears which becomes the only maximum for  $R \gtrsim 500$ . It lies around  $t_{\max} \approx 9$ . We have no evidence for a further increase of  $t_{\max}$  as  $R$  increases, but it cannot be excluded on the basis of these data.

Let us now discuss the behavior of the energy spectrum. For early times  $t \lesssim 3$ , spectra of the large  $R$  viscous computations are essentially identical to those of the inviscid flow. At later times, however, the high- $R$  runs lead to nearly isotropic high-wave-number behavior, in which the effect of the initial condition is largely forgotten. In Fig. 5, energy spectra are plotted for  $R = 1600$  at  $t_{\max} = 9$  and for  $R = 3000$  at  $t_{\max} = 9$  and at  $t = 5$ . Especially, for the  $R = 3000$  case, the log-log plot of  $E(k)$  shows a rather obvious power law character, although inertial and dissipation range have considerable overlap. In order to extract such quantities as power law exponents and dissipative cutoff wave numbers we again use least-squares fits to Eq. (8). The results are indicated as solid lines in Fig. 5. Results for

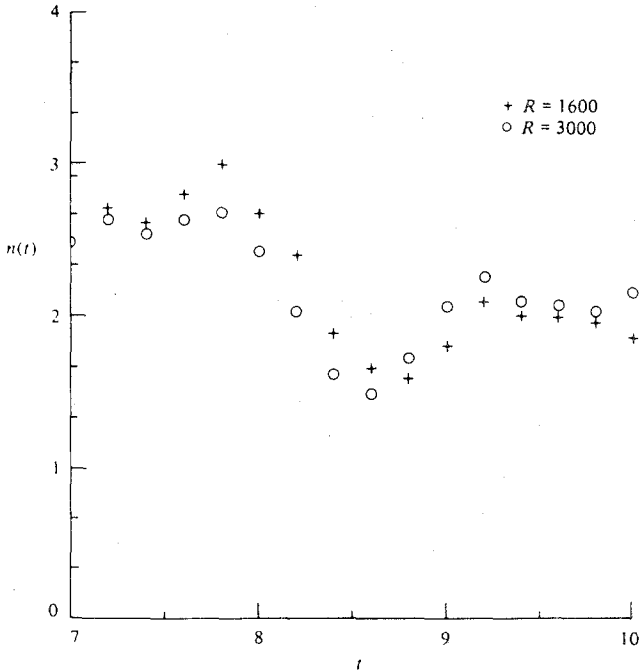


Fig. 6. Exponent  $n(t)$  of the algebraic factor vs.  $t$  in the spectral fit (8). The least-squares fits are done over the wave-number interval  $13 < K < 83$ . The plus signs are for  $R = 1600$ ; the circles are for  $R = 3000$ .

the exponent  $n(t)$  are plotted in Fig. 6 for both  $R = 1600$  and  $R = 3000$ . It is apparent that around  $t = 8$ ,  $n(t)$  drops quickly from a value of the order 3 to a value close to 2. Also, it can be seen that  $n(t)$  has a minimum value close to the Kolmogorov value; this occurs in the vicinity of  $t_{\max}$  when the dissipation rate is maximum.

Let us finally discuss results concerning intermittency of the small scales. Direct access to intermittency is provided by analyzing the fluctuations of local dissipation, which is defined by

$$\begin{aligned} \epsilon(\mathbf{r}) &= \nu \sum_{ij} e_{ij} e_{ij} \\ e_{ij} &= \frac{1}{2} \left( \frac{\partial}{\partial r_i} V_j + \frac{\partial}{\partial r_j} V_i \right) \end{aligned} \tag{10}$$

Consider the fluctuations in the local dissipation  $\tilde{\epsilon}(\mathbf{r}) = \epsilon(\mathbf{r}) - \bar{\epsilon}$ . Ac-

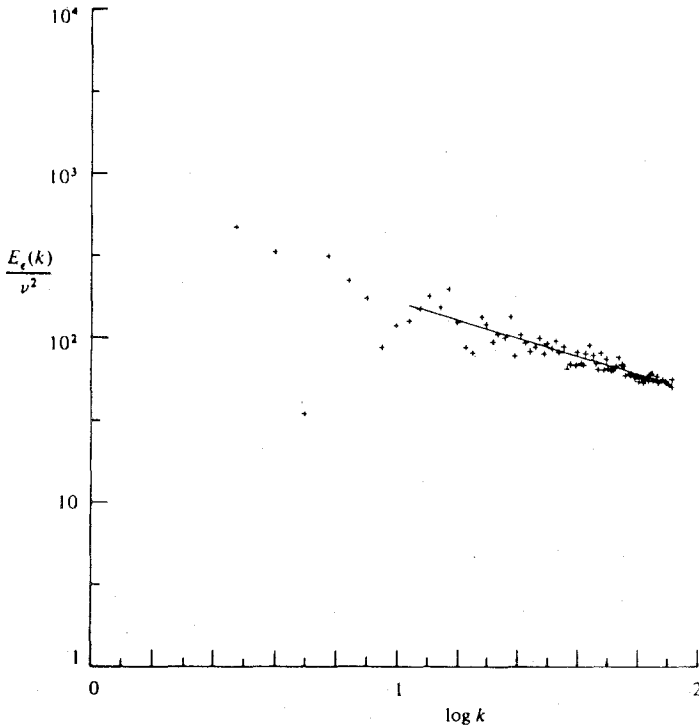


Fig. 7. Plot of the spectrum of dissipation fluctuations  $\epsilon'(r) = \nu \omega^2(r)$  for  $R = 3000$  at  $t = 9$ . The solid line is a least-squares fit to the form (11) over wave numbers  $11 < k < 83$ . The least-squares result is  $\mu = 0.46$  in (11).

ording to the original Kolmogorov theory, at inertial-range scales these fluctuations are expressible in terms of velocity fluctuations. These contribute a self-similar process with exponent  $1/3$ .<sup>(7)</sup> Hence, the spectrum of dissipation fluctuations  $E_\epsilon(k)$  is given, at inertial range wave numbers, by  $E_\epsilon(k) \sim \nu^2 \bar{\epsilon}^{4/3} k^{5/3}$ . In contrast, according to the modified Kolmogorov theory,<sup>(4)</sup> dissipation fluctuations may be correlated over distances much larger than the viscous cutoff scale  $l_D$ . Modified Kolmogorov theory then leads to

$$E_\epsilon(k) \sim \bar{\epsilon}^2 (kl_0)^{-1+\mu} \quad (11)$$

where  $\mu$  is an exponent which in some models allows a geometric interpretation, as the codimension of a fractal on which dissipation is concentrated.<sup>(5,6)</sup>

As a measure of local dissipation we have analyzed the quantity  $\epsilon^1(r) = \nu \omega^2(\mathbf{r})$  where  $\omega(\mathbf{r})$  is the vorticity. In Fig. 7 we plot the spectrum  $E_\epsilon(k)$  for  $R = 3000$  at  $t = 9$  near the time of maximum dissipation. A least-squares fit to a form analogous to Eq. (8) leads to a value

$$\mu = 0.5 \pm 0.2 \quad (12)$$

consistent with experimental data.<sup>(21)</sup> It has been conjectured<sup>(5)</sup> that in the limit  $\nu \rightarrow 0$ , all the dissipation will be concentrated in a fractal. In our calculation at  $R = 3000$  power-law behavior is only observed in the highest-wave-number octave. This corresponds to about one mesh unit in physical space and therefore we cannot expect to actually see fractal-like structures in the flow.

#### 4. SUMMARY

Direct numerical integration of the Navier–Stokes equation has been used in order to investigate small-scale behavior of both inviscid and viscous flow. For the largest Reynolds numbers accessible to our spatial resolution we have started to observe Kolmogorov-like power law behavior of the energy spectrum. This occurs around the time of maximum energy dissipation rate.

We have compared results based on direct integration of the Euler equation and on temporal power series to study the question of the existence of a real time singularity in the inviscid flow. No definitive conclusion can be drawn since there exists conflicting evidence. The “noise” observed in Padé analysis may suggest a very complicated analytic structure possibly related to the existence of a natural boundary.

## ACKNOWLEDGMENTS

We would like to thank A. T. Patera for assistance with the algorithms and design of the spectral time-integration code. The work has benefited from conversations with R. H. Kraichnan, B. Mandelbrot, W. V. R. Malkus, R. L. McCrory, R. Pellat, P. L. Sulem, and J. Weiss. Also we would like to thank N. T. Jones, Jr., for considerable assistance with the graphics. He also made a striking computer generated ciné film of the Taylor–Green vortex. Computations were done in part on a Cray-1 at the National Center for Atmospheric Research, which is sponsored by NSF, and in part on an Amdahl V/5 at the University of Guelph. U. Frisch, B. G. Nickel, and R. H. Morf would like to acknowledge the hospitality of the Department of Physics at Harvard University, where much of this work was done.

## REFERENCES

1. E. N. Lorenz, *J. Atmos. Sci.* **20**:130 (1963); D. Ruelle and F. Takens, *Commun. Math. Phys.* **20**:167 (1971); **23**:343(E) (1971).
2. A. N. Kolmogorov, *C. R. Acad. Sci. USSR* **30**:301 (1941).
3. G. K. Batchelor and A. A. Townsend, *Proc. R. Soc. London Ser. A* **199**:238 (1949).
4. A. N. Kolmogorov, *J. Fluid Mech.* **13**:82 (1962).
5. B. Mandelbrot, in *Turbulence and Navier–Stokes Equation*, R. Temam, ed., Lecture Notes in Mathematics, Vol. 565 (Springer, Berlin, 1976), p. 121.
6. U. Frisch, P. L. Sulem, and M. Nelkin, *J. Fluid Mech.* **87**:719 (1978).
7. U. Frisch, in Les Houches, Session XXXVI, *Chaotic Behaviour in Deterministic Systems*, 1981, G. Iooss, R. H. G. Helleman, and R. Stora, eds. (North Holland 1983).
8. R. H. Kraichnan, *Phys. Fluids* **10**:2080 (1967).
9. U. Frisch and R. Morf, *Phys. Rev. A* **23**:2673 (1981).
10. P. G. Saffman in: *Topics in Non-Linear Physics*, N. Zabusky, ed. (Springer, Berlin, 1968), p. 485.
11. G. I. Taylor and A. E. Green, *Proc. R. Soc. London Ser. A* **158**:499 (1937).
12. M. E. Brachet, D. I. Meiron, S. A. Orszag, B. G. Nickel, R. H. Morf, and U. Frisch, *J. Fluid Mech.* **130**:411 (1983).
13. R. H. Morf, S. A. Orszag, and U. Frisch, *Phys. Rev. Lett.* **44**:572 (1980).
14. R. H. Morf, S. A. Orszag, D. I. Meiron, U. Frisch, and M. Meneguzzi, in *Proc. 7th Intl. Conf. on Numerical Methods in Fluid Dynamics*, R. W. McCormack and W. C. Reynolds, eds., Lecture Notes in Physics, Vol. 141 (Springer, Berlin, 1981), p. 292.
15. W. Wolibner, *Math. Z.* **37**:698 (1933).
16. G. A. Baker, *Essentials of Padé Approximants* (Academic, New York, 1975).
17. M. E. Fisher and M. Au-Yang, *J. Phys. A* **12**:1677 (1979); **13**:1517 (1980).
18. C. Sulem, P. L. Sulem, and H. Frisch, *J. Comp. Phys.* **50**:138 (1983).
19. Y. F. Chang, M. Tabor, and J. Weiss, *J. Math. Phys.* **23**:531 (1982).
20. J. Weiss, Analytic Structure of Hénon–Heiles System, in *Mathematical Methods in Hydrodynamics*, A.I.P. Conf. Proc. No. 88 (AIP, New York, 1982).
21. A. S. Monin and A. M. Yaglom, *Statistical Fluid Mechanics* Vol. 2 (MIT Press, Cambridge, Massachusetts, 1975).